5.1. Introduction

Research based on structurally manipulated DNA (Deoxyribonucleic acid) either as additive or as template for organic polymers have been one of the top priorities among the researchers who are working especially in the field of biosensors and molecular electronics applications [Livshits et al. (2014), Surin et al. (2016), Beratan et al. (2016), Bang et al. (2016), Sumathi et al. (2016), Gupta et al. (2011), Watson et al. (2014)]. There are enough works which have yet been published, showing that DNA conducts electronic transport up to a short length by hoping and tunnelling mechanisms which has also discussed in the present work with the help of diode as it has considered as the basic building block of electronic devices [Qian et al. (2017), Dekker et al. (2001), Porath et al. (2000), Periasamy et al. (2016)]. The introduction of DNA into semiconducting organic polymers might be a choice to improve some common issues associated with the organic semiconductors like stability, thermal degradation and mobility. For example, DNA is being studied in semiconductor devices, such as Schottky diodes and sensors devices widely for its utilization and application [Al-Ta'ii et al. (2015), Al-Ta'ii et al. (2016), Shi et al. (2006)].

The DNA molecule comprises of pentose sugar, phosphate group and four bases- namely, adenine (A), guanine (G), cytosine (C) and thymine (T) [Rakitin et al. (2001)]. These bases arrange carefully to form highly effective hydrogen bonds with each another in such a way that A is always bonded to with T and G is always bonded to C within the helices while phosphate groups flanked out the helices [Dekker et al. (2001)]. DNA, when used as a molecular wire, has shown a nonlinear response in *I–V* characterization [Khatir et al. (2015)]. In addition, the electron transfer through such molecular wires and DNA strands have been modeled as donor-bridge-acceptor systems owing to their excellent analogy.

These wires enable charge transport activity as rectifiers, transistors, or switches when MDM (metal-DNA-metal) sandwiches are fabricated [Khatir et al. (2015), Joachim et al. (2004)]. That is why; the structure of DNA has been considered as an ideal for electron transfer due to overlapping of electron orbitals of some bases with another one, along the axis of molecule. For example, it has been assumed that hole is more stable on a G—C base pair of a DNA molecule than that of A-T base pair. In these circumstances, a hole localizes on a particular G—C base pair and hence electron and hole are able to shuttle via coherent tunneling (short range electron transfer) and diffusive thermal hopping (long range electron transfer) processes [Dekker et al. (2001), Porath et al. (2000), Taniguchi et al. (2006), Korol et al. (2016), Rawtani et al. (2016), Lewis et al. (2002), Beratan et al. (2014), Giese et al. (2001), Xiang et al. (2015), Kleine-Ostmann et al. (2006)]. Recently a new mechanism called *"hot-hole transfer"* for long range charge conduction in DNA by the use of powerful donor system has been reported. According to this mechanism, donor system is capable to inject charge carriers into nearby nucleotide bases which accelerate the transfer rates [Beratan et al. (2016)].

In view of above, we intentionally synthesized G-C rich single as well as double strand DNA with the help of vendor, in order to study the charge transport properties when incorporated into p-type rr-PQT-12, (conducting polymer, supports hole transport). Meanwhile, this polymer has also a capability to donate electrons due to presence of electron rich hetero-atoms [Singh et al. (2017)]. Similarly, for the proper intimacy of DNA with polymer; modified DNAs are used as template to aggregate rr-PQT-12 in chloroform solvent using our optimized protocol [Singh et al. (2017)]. The rr-PQT-12 is a well-known heterocyclic conducting polymer with repeating unit of planner quarter thiophene on its

backbone due to presence of dodecyl groups [Singh et al. (2017)]. These groups make it excellent towards better processability and proper aggregation (interdigitations via alkyl chain) in non-aqueous solvents like chloroform, toluene etc. at a given conditions.

5.2. Experimental

5.2.1 Materials

Calf Thymus (Natural) DNA (ct-DNA ~40% GC pair) was purchased from Sigma Aldrich, USA and used without purification. rr-PQT-12 (ADS12PQT, Lot#14K007B1, molecular weight =15,000–50,000 & HOMO = 5.24 eV & LUMO = 2.97 eV) was purchased from American Dye Source, Inc. USA. Chloroform was purchased from Merck, India and used as such. All chemicals have been used of analytical grade without further purification.

As-synthesized ss-DNA and ds-DNA having enriched G-C pairs (84.8%) was purchased from Integrated DNA Technology, IDT, India and used as received. The G-C variants in ss-DNA and ds-DNA sequence are as follows-

5′-GTCGCGTCGCGTCGCGCGTCGCGCGCTGCGCGCGCGTCGCGCGCTC3′
(ss-DNA);
5’-CAGCGCAGCGCAGCGCGCAGCGCGCGACGCGCGCGCAGCGCGCGAG-3’
3’-GTCGCGTCGCGTCGCGCGTCGCGCGCTGCGCGCGCGTCGCGCGCTC-5’
(ds-DNA)

5.2.2 Optimization of DNA guided rr-PQT-12 fibril formation

The DNA-DDAB complexes were formed by allowing electrostatic interactions between negatively charged phosphate groups (DNA) and positively charged quaternary ammonium group (DDAB) in aqueous solvent using the following manner, in which equimolar mixture of DDAB solution was added to as-received DNAs.

Natural ds-DNA-DDAB complex was prepared by addition of 200µL ds-DNA (calf thymus) (from 200, 400 and 800 µM natural ds-DNA stock solution) and 200µL DDAB and designated as 'ND'. Similarly, three different concentrations of G-C rich ss-DNA-DDAB complexes were prepared by addition of 200µL ss-DNA (from 200, 400 and 800µM ss-DNA stock solution) and 200µL DDAB. All these samples are designated as 'S2', 'S4' and 'S8' respectively. Similar approach was adopted for the preparation of G-C rich ds-DNA-DDAB complex and they are designated as 'D2', 'D4' and 'D8' respectively throughout the manuscript.

We observed that a white precipitation of DNA-DDAB complexes were formed upon mixing of individual components due to interaction of negatively charged phosphate and positively charged amino group of DDAB. All complexes were centrifuged, washed severally and vacuum dried for three days at room temperature. Thereafter, DNA-DDAB complexes were again tested for their dissolution in chloroform and preserved in vacuum for the further experimentation.

Preparation of DNA-DDAB/rr-PQT-12composite:

Homogenous solutions of DNA-DDAB/rr-PQT-12 composites were prepared by addition of various DNA-DDAB complexes (as mentioned above) and 300µL rr-PQT-12 (0.5% by weight in chloroform). After that the as-prepared solutions were kept in mixer vibrator for

10 h to ensure the complete dissolution and further used for device fabrication. Thus we have prepared seven composites viz. ND/rr-PQT-12, S2/rr-PQT-12, S4/rr-PQT-12, S8/rr-PQT-12, D2/rr-PQT-12, D4/rr-PQT-12 and D8/rr-PQT-12. These composites were aged for 45 minutes followed by heating to insure their corresponding fibrous composites.

5.3 Results and discussion

It is well known that solvent homogeneity is one of the conditions for the orientation of individual components (e.g. polymer over DNA template). The nature of substrate plays decisive role for the orientation of polymers like rr-P3HT or rr-PQT-12. For example, OTS treated SiO_2 substrate (hydrophobic nature) favours edge-on orientation while hydrophilic substrates favour face-on orientation of rr-PQT-12 [Pandey et al. (2017)].

With the same concept, DNA-DDAB complex is used in order to make it compatible with rr-PQT-12 in chloroform (proper interaction of dodecyl end-group of DDAB with hexyl end-group of rr-PQT-12 as shown in Fig. 5.1 (I)). In fact this evidence is exemplified by photoluminescence (PL) spectroscopy as discussed latter in the manuscript. On the other hand, in aqueous state, DNA interacts via its negatively charged phosphate end-group to the positively charged DDAB during complex formation and give white precipitate of DNA-DDAB (as shown in photograph of inset of Fig. 5.2). Thus surface of DNA is now hydrophobic in nature that preferably allows edge-on interaction of polymer as shown in Fig. 5.1 (II) below. Similarly, as soon as time passes, the colour of solution mixture containing DNA-DDAB/rr-PQT-12 turns reddish-brown from orange colour that shows the evidence of fiber formation similar to our earlier work [Singh et al. (2017)]. The evidence of DNA-DDAB/rr-PQT-12 solution mixture into its fibrous form was ascertained

by UV visible, photoluminescence (PL) spectroscopy, transmission electron microscopy (TEM) and atomic force microscopy (AFM) as explained below.

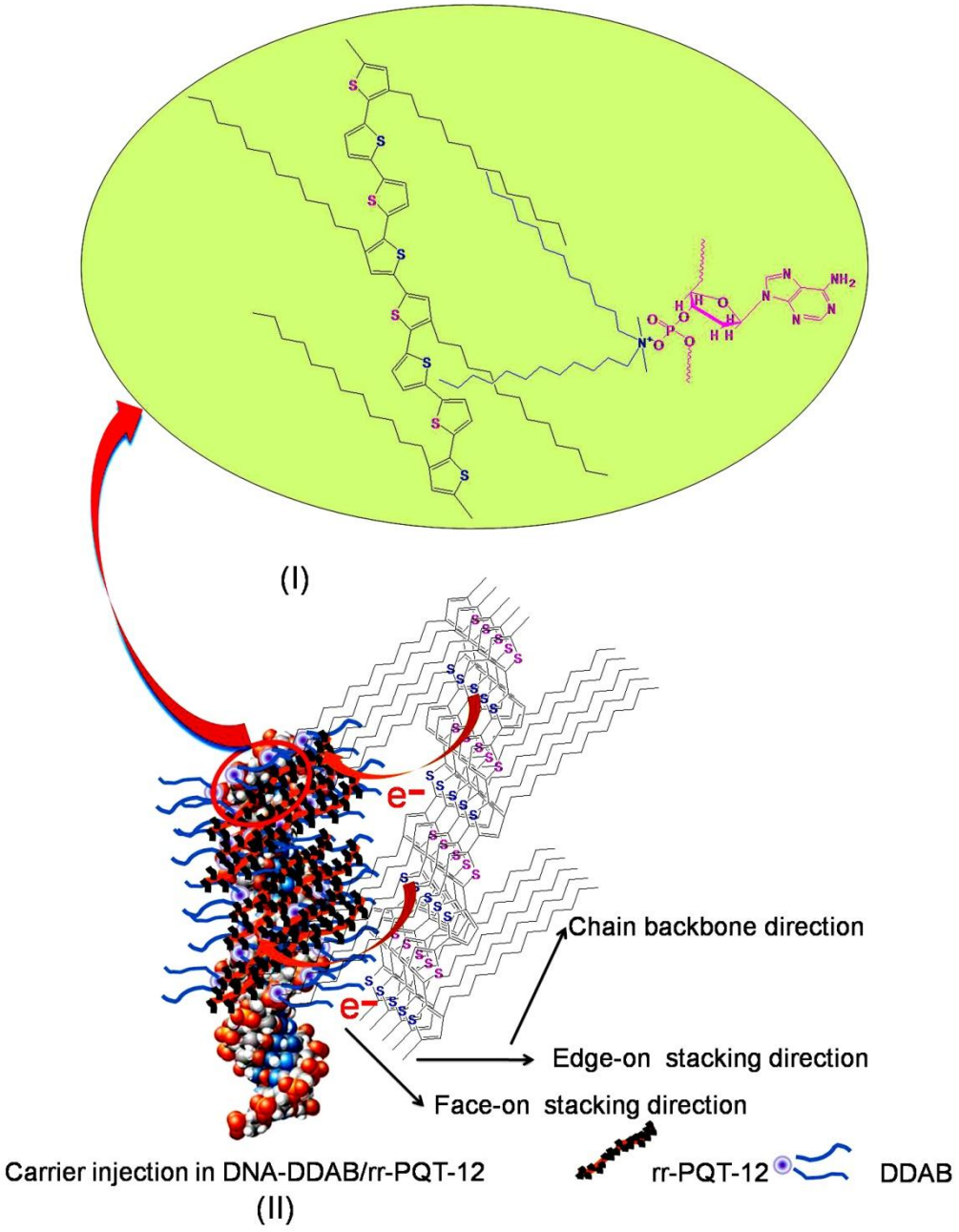

Fig. 5.1. (I) Chemical interactions of DNA, DDAB and rr-PQT-12 in DNA-DDAB/rr-PQT-12 fiber and (II) possible assembly of rr-PQT-12 over DNA-DDAB complex.

Structural study: UV-visible and PL spectroscopy:

The existence of ss-DNA, ds-DNA and DDAB onto the rr-PQT-12 fibers were ascertained by UV-visible spectroscopy (EPOCH2C, Biotech Instrument Inc., USA) analysis (as shown in Fig. 5.2. Generally, DNA gives its characteristics peaks at 260 nm and 331 nm due to corresponding purine and pyrimidine bases respectively [Rittman et al. (2012)], while DDAB exhibit an absorption peak at 280 nm [Mehta et al. (2008)]. However in our case (S2/rr-PQT-12 and D2/rr-PQT-12), we observe broad peak around 265 nm due to overlapping of DNA and DDAB peak. On the other hand, the absorption peak at 473 nm and a shoulder peak at 603 nm are arising due to π-π* transition and coupling of π-π* transition to the C=C stretching respectively in the planer thiophene ring of rr-PQT-12 [Singh et al. (2017), Kumar et al. (2014)]. Except the absorption intensity, we observed almost similar peak positions for other complexes and their respective composites. It means that all as-prepared composites are turned into fibrous form under the specified conditions (as discussed in preparation of composition section above).

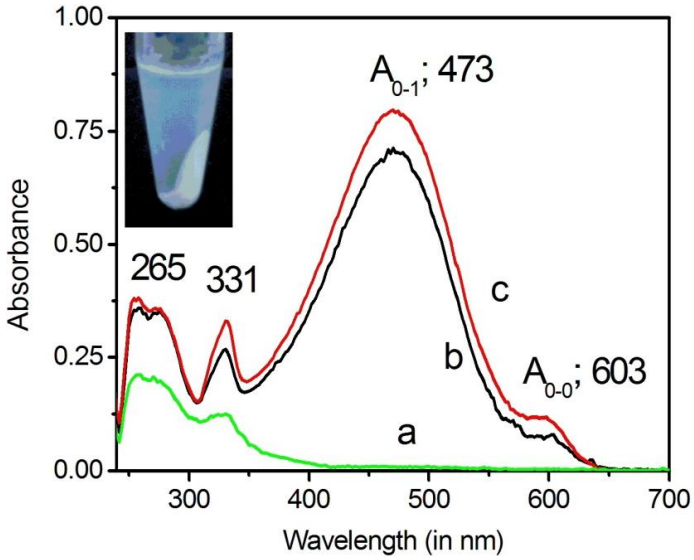

Fig. 5.2. UV visible spectra of (a) D2, (b) S2/rr-PQT-12 and (c) D2/rr-PQT-12 in chloroform. Inset shows white precipitate of D2.

The confirmation of aggregation type was further exemplified by photoluminescence emission (PL) spectrophotometer (Perkin Elmer, LS-50B, USA), excited at 475 nm for similar concentrations of rr-PQT-12, S2/rr-PQT-12 and D2/rr-PQT-12 solutions (shown in Fig. 5.3). The marginal increment in the emission intensities has been seen from rr-PQT-12→ S2/rr-PQT-12→ D2/rr-PQT-12. It might be due to large numbers of charge transfer taking place from modified DNA to aggregated polymer [Singh et al. (2018)]. The packing and molecular orientation in as-prepared dispersions (S2/rr-PQT-12 and D2/rr-PQT-12) is expected prominently along face-on direction along with weak edge-on aggregation similar to rr-PQT-12.

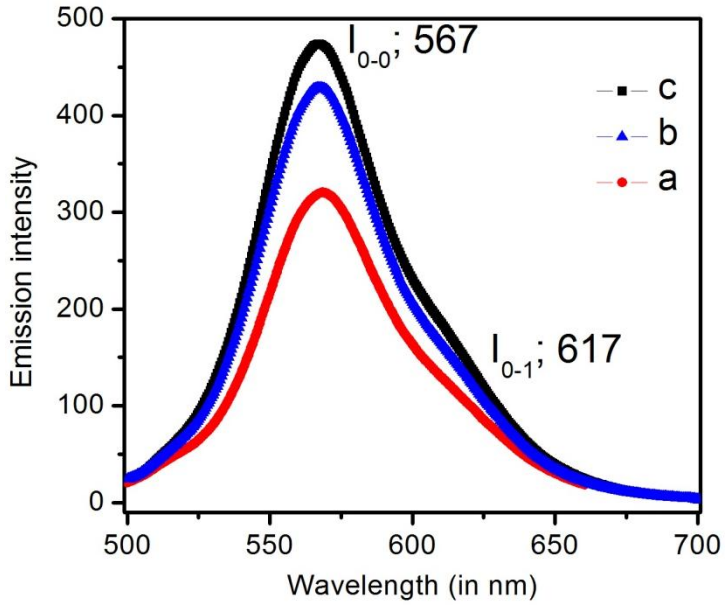

Fig. 5.3. PL spectra of (a) rr-PQT-12, (b) S2/rr-PQT-12 and (c) D2/rr-PQT-12 solutions. (λ_{ex} = 475 nm).

To insure the interactions and charge transfer phenomenon, time resolved emission study was performed. Herein, equal concentrations of as-prepared fiber dispersions (as described in sec. 2.3) rr-PQT-12, S2/rr-PQT-12 and D2/rr-PQT-12 were used in order to

confirm the mechanism of interaction. Fluorescence decay profiles of all these samples were recorded on Edinburg FLS 900 fluorescence spectrophotometer (Edinburg Instruments, UK) using the time correlated single photon counting (TCSPC) technique. The excitation source was light emitting diode (LED) with a low full width at half maximum at wavelengths ~ 369 nm. These systems were found to contain two different life-times when excited at ~369 nm. The decay profile and the different parameters observed for rr-PQT-12, S2/rr-PQT-12 and D2/rr-PQT-12 are depicted in Fig. 5.4 and Table 5.1 respectively. If interaction takes place in the ground state the life time should remain unchanged [Pandey et al. (2014), Singh et al. (2018)]. The changes in the life time happen when interaction occurs in the excited state. From Table 5.1, it is clear that the life times associated with S2/rr-PQT-12 and D2/rr-PQT-12 are different in comparison to that of rr-PQT-12. It clearly resembles that the interaction between S2- or D2-complex with rr-PQT-12 is taking place in the excited state and hence the charge transfer is also taking place in the excited state [Pandey et al. (2014)]. The decay curves at excitation wavelength 369 nm were analyzed in terms of the multi-exponential model in the following form (eq.1 and eq. 2)-

$$I(t) = \sum B \exp(-t/\tau) \quad (1)$$

where, B is amplitude and τ is decay time. Here, a two component analysis as given below was found to be suitable for each of these cases.

$$I = B1 \exp(-t/\tau_1) + B2 \exp(-t/\tau_2) \quad (2)$$

where, B1 and B2 are the respective amplitudes and τ_1 and τ_2 are the respective decay times.

The values of B and τ were determined by nonlinear least squares impulse reconvolution analysis with the goodness of the fit judged by the residuals, autocorrelation function and χ^2 (Table 5.1). The measurement error in the decay time is of the order of 0.01 in the nanosecond range.

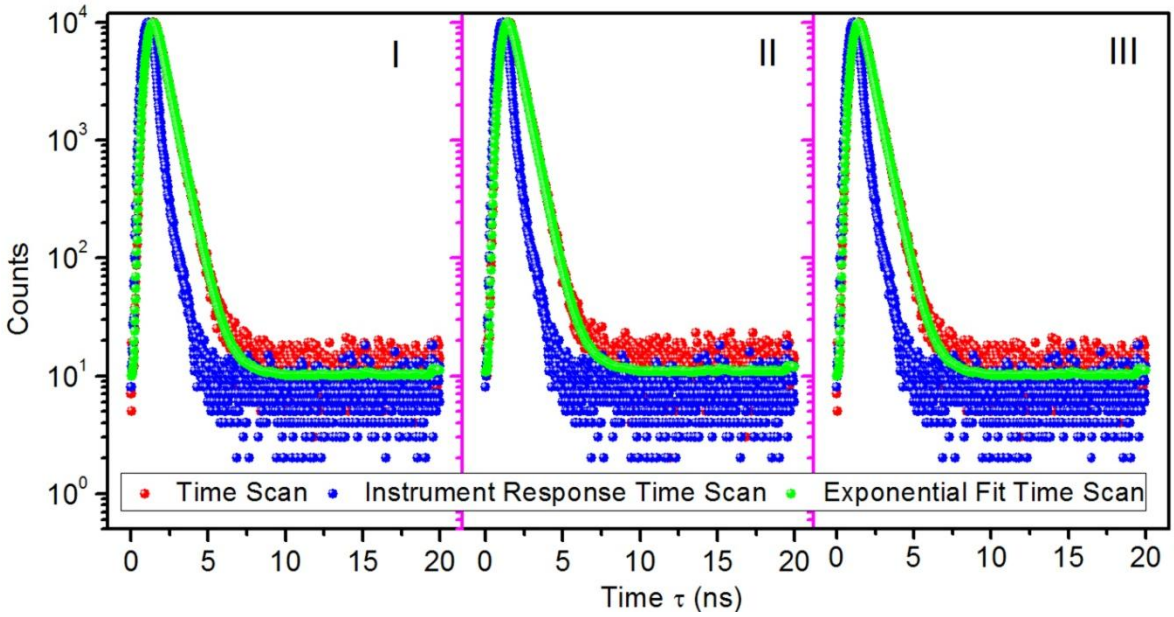

Fig. 5.4. Time resolved florescence decay curves of (I) rr-PQT-12, (II) S2/rr-PQT-12 and (III) D2/rr-PQT-12 solutions. (λem = 369 nm).

Morphological study:

The evidence of fiber formation was further exemplified by TEM (FEI Techai, (G2 F20 twin, Swiss Republic) and AFM (NT-MDT, NTEGRA Prima, Russia) (shown in Fig. 5.5). From TEM image, it can be concluded that both S2/rr-PQT-12 and D2/rr-PQT-12 are assembled successfully into fibrous form. These are semi-crystalline in nature and exhibit its characteristics Bragg diffraction patterns corresponding to (100), (200) and (010) planes for both S2/rr-PQT-12 and D2/rr-PQT-12 fibers (shown in selected area electron diffraction, SAED pattern of Fig. 5.5(c) and Fig. 5.5(d)) [Singh et al. (2017), Wang et al.

(2013)]. It means that rr-PQT-12 self-assembled together over either type of DNAs into its favourable direction. Thereafter, with the help of AFM, the expected orientation and the S2- and D2-complex behavioural response with polymers were exemplified. On comparing both the AFM images, irrespective of DNA type into S2 and D2 complex (prepared from ss- and ds-DNA with DDAB), S2/rr-PQT-12 and D2/rr-PQT-12 fibers have almost equal diameters (average) 103 nm and 105 nm respectively (*cf.* Fig. 5.5e and Fig. 5.5f). It means both complexes exhibit similar behavioural as template for aggregation of rr-PQT-12 under given conditions.

The surface potential imaging of S2/rr-PQT-12, D2/rr-PQT-12 and rr-PQT-12 fibrous films (200nm) spin casted over silicon substrate (1cm × 1cm) were compared by Kelvin probe force microscopy (KPFM) along with AFM using Si coated Pt-tip (work function= 5.69 eV, biased at 3.0 V). In this technique, film surfaces were randomly selected and targeted for the study of variation in surface potentials, topographic and their respective phase image as shown in Fig. 5.6 . From KPFM image, it is clear that the surface potential is increased by approximately 5 times (120-130 mV in case of D2/rr-PQT-12) and ~2 times (50-55 mV in case of S2/rr-PQT-12) with respect to pure polymer (20-25 mV in case of rr-PQT-12) surface (*cf.* Fig. 5.6 (a), Fig. 5.6 (b) and Fig. 5.6(c)). This is due to larger number of charge transfer via favorable hopping from hydrogen bonded G-C pair to another G-C along the rigid strands of ds-DNA translated to aggregated polymer, while this phenomenon is less effective in case of ss-DNA due to absence of nucleotide chain rigidity. This evidence can also be seen in case of junction property study (as discussed latter).

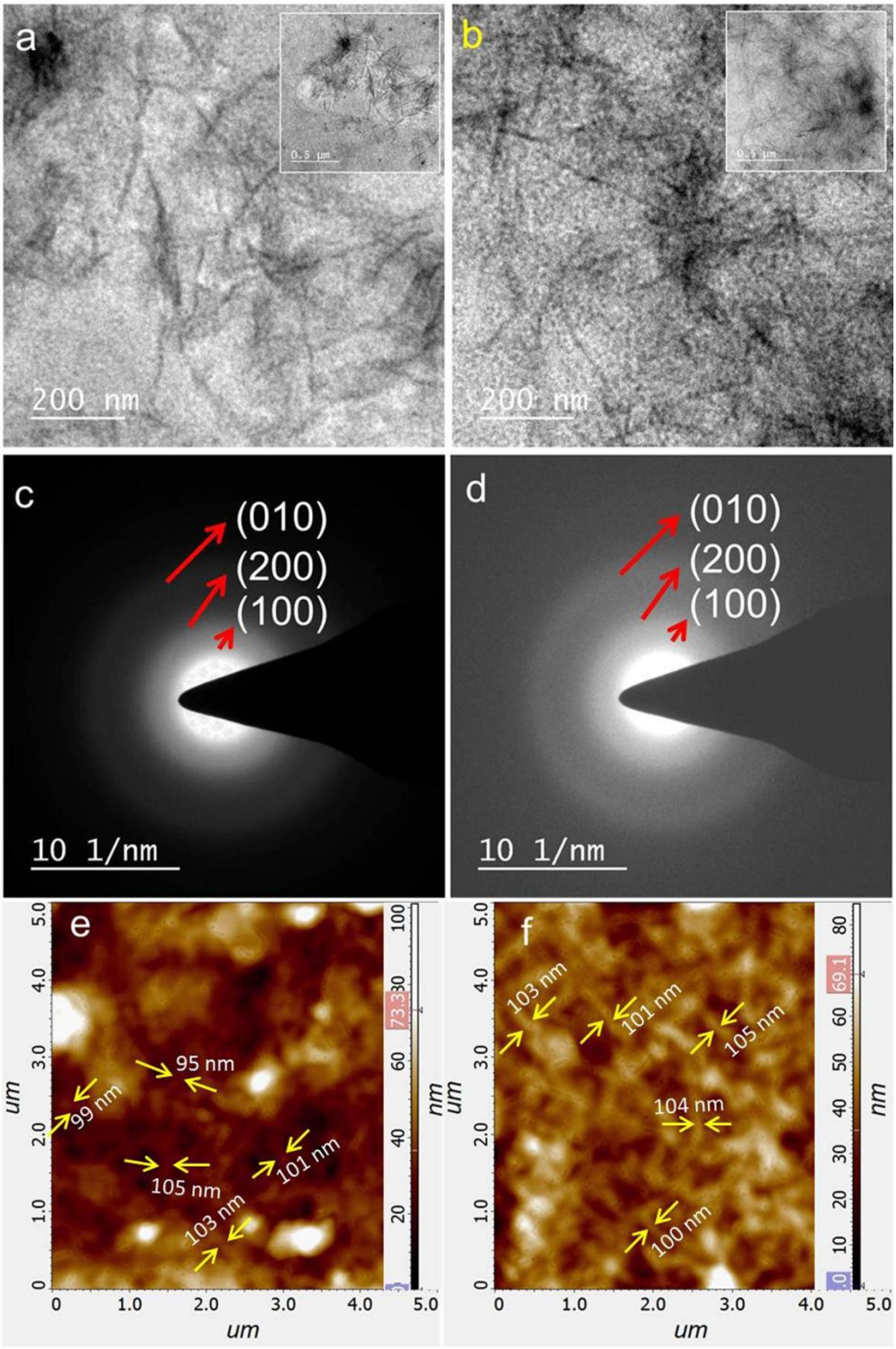

Fig. 5.5. TEM image (a & b), SAED pattern (c & d) and AFM image (e & f) of S2/rr-PQT-12 and D2/rr-PQT-12.

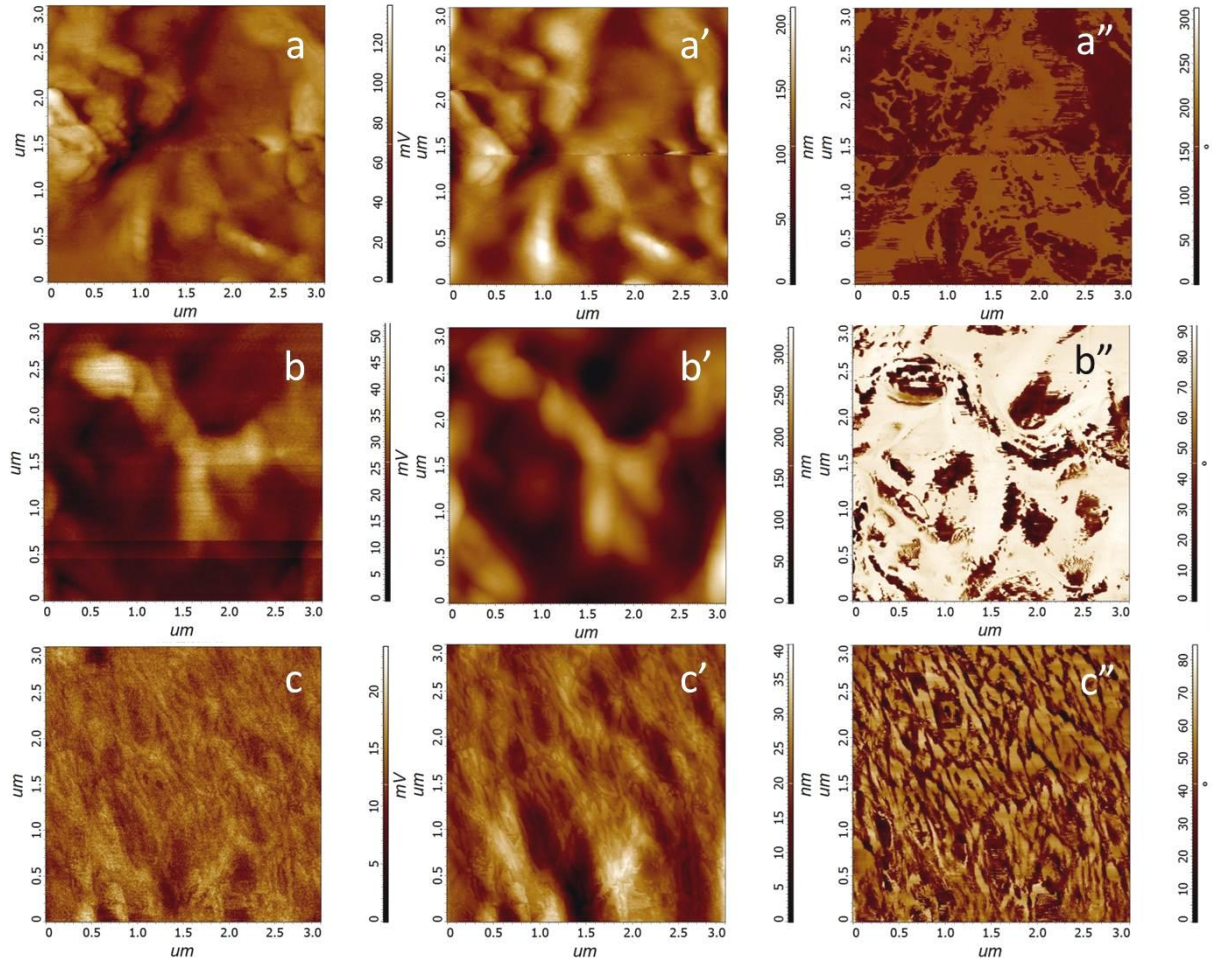

Fig. 5.6. KPFM and AFM (in topographic and their phase image) of D2/rr-PQT-12 (a, a'& a''), S2/rr-PQT-12 (b, b' & b'') and rr-PQT-12 (c, c'& c'') respectively.

Fabrication of device and study of charge transport properties:

Indium-doped tin oxide (ITO) coated glass (with surface resistance of 12 Ω-cm^2) substrate was used as the bottom electrode for the formation of Schottky diode (vertical diode). This substrate was properly cleaned by 30 min ultra-sonication followed by multiple washing using DI water, acetone, propanol, and methanol subsequently. After that, 20μL of all as-aged composite solutions were spin coated on the cleaned ITO substrate at a spin rate of 1500 rpm for 40s followed by 3000 rpm for 30s. As-deposited films were

vacuum dried at 50^0 C for 1h in N_2 atmosphere. Finally, aluminium contacts (dots of diameter=1mm and thickness=120nm) were deposited over the film as top electrode of the Schottky contact using thermal evaporation unit (Model no.12A4D, Hind High Vacuum Bangalore, India) with vacuum level of 5×10^{-6} Torr and a deposition rate ~1.7 Å/Sec.The electronic properties of as-fabricated devices with Al/DNA-DDAB/rr-PQT-12/ITO configuration were studied with the help of current density *vs.* voltage (J–V) characteristics using probe station (Everbeing, RF Probe Station, Model no. PE-4RF, Taiwan) and Keithley 2612A dual channel system source meter at the room temperature (300 K) under dark conditions in ambient.

In general interpretation, polyalkylthiophenes-metal contacts; where the metal is chosen with low work function than that of polymer, the J-V characteristics exhibited by them are much closely (but not exactly) analogous to Schottky behavior observed in conventional semiconductors. In which, it has been assumed that, tunneling process through barrier in series with the thermally activated bulk conductivity produced through hopping process in polymer are responsible for such type of electron transition activities, which is more closely to a thermionic emission process in series with the bulk conductivity observed in conventional semiconductors [Tomozawa et al. (1989), Bredas and Silbey (2012)]. That is why, the junction behaviors parameters is being represented directly using thermionic emission theory for numerous devices fabricated using metal-polymer contacts [Singh et al. (2010), Sze (1981)]. The J-V characteristics of as-fabricated diodes based on rr-PQT-12, ND/rr-PQT-12, ss-DNA-DDAB/rr-PQT-12 and ds-DNA-DDAB/rr-PQT-12 is shown in the Fig. 5.7. It is clear that the charge transport property of ND/rr-PQT-12 is much poor (even on elevated potential i.e. ±3V) as compared to that of rr-PQT-12 (*cf.* Fig. 5.7 (I & II)). This

is due to the insulating nature of natural DNA (low G-C content). (*Note: Since we were unable to measure the charge transport properties of composites formed using addition of natural ds-DNA-DDAB complexes containing 400 µM and 800 µM ds-DNA due to highly insulating nature of natural ds-DNA. That is why we discarded these as-prepared composites).* On comparing the charge transport behavior of ND/rr-PQT-12, rr-PQT-12, ss-DNA-DDAB/rr-PQT-12 and ds-DNA-DDAB/rr-PQT-12, both ss-DNA-DDAB/rr-PQT-12 and ds-DNA-DDAB/rr-PQT-12 exhibit better charge transport characteristics than that of ND/rr-PQT-12 or even rr-PQT-12 alone (*cf.* Fig. 5.7 (I), Fig. 5.7 (II) and Fig. 5.7 (III)). It might be due to the contribution of localized charges present in G-C rich DNAs with as-associated rr-PQT-12. The forward current behavior increases with the addition of ss-DNA-DDAB complex with respect to that of rr-PQT-12 alone. However, it decreases from S2→S4→S8 due to increase in G-C contents causes increase in barrier height. Similar trend can be also observed in case of D2→D4→D8 (as shown in inset of Fig. 5.7 (III)). It means that higher concentration of DNA molecules could hindered the charge transport and can only aid charge transport if used in optimal concentrations with rr-PQT-12. However, ds-DNA-DDAB/rr-PQT-12 exhibit better rectification behavior than that of ss-DNA-DDAB/rr-PQT-12 in either case of DNA contents. This is due to more favorable hopping from hydrogen bonded G-C pair to another G-C along the rigid strands of ds-DNA, while this phenomenon is not possible in case of ss-DNA due to lack of nucleotide chain rigidity.

Various parameters like barrier height, saturation current density, ideality factor, rectification ratio and current density ratio have been evaluated for all as-fabricated diodes based on the assumption in which, the current is due to thermionic emission, the relation

between the applied forward bias and current density, $J=I/A$ can be expressed as [Rhoderick and Williams (1988)]-

$$J = J_0 exp\left(\frac{qV}{\eta kT}\right)\left[1 - exp\left(\frac{-qV}{kT}\right)\right] \quad (3)$$

For $V>3kT/q$ the equation (3) can be written as-

$$J = \frac{I}{A} = J_0 exp\left(\frac{qV}{\eta kT}\right) \quad (4)$$

Where, η is the ideality factor, T is the temperature in Kelvin, q is the electronic charge, k is the Boltzmann constant and J_0 is the reverse saturation current which has been achieved by extrapolating the straight line of lnJ to intercept the axis at zero voltage.

The reverse saturation current J_0 can be expressed as-.

$$J_0 = A^* T^2 exp\left(\frac{-q\Phi_B}{kT}\right) \quad (5)$$

Where, A is the effective diode area which is equal to 7.85×10^{-3} cm^2 in our case, $A^*$is the effective Richardson constant which is equal to 120 A $cm^{-2}K^{-2}$ and Φ_B is the zero-bias barrier height which can be extracted from (5) as-

$$\Phi_B = \frac{kT}{q}\ ln\left(\frac{A^* T^2}{J_0}\right) \quad (6)$$

Ideality factor, a parameter which is normally used to measure the deviation of practical diodes from ideal thermionic emission model and can be extracted from slope of the linear region of the lnJ-V plot and can be written from (4) as-

$$\eta = \frac{q}{kT}\left(\frac{\delta V}{\delta(ln\, J)}\right) \quad (7)$$

All the parameters calculated using above relationships are tabulated in the Table 5.2. For the case of ITO/ND/rr-PQT-12/Al device, barrier height (Φ_B) (calculated from eq. (6)) is more than that of ITO/rr-PQT-12/Al (*i.e.* 0.789±0.038 *vs.* 0.705±0.045). This is due

of smaller value of saturation current density (J_0). Similarly, the ideality factor (η) (calculated from eq. (7)) and rectification ratio (RR) of ITO/ND/rr-PQT-12/Al is also observed much poor due to improper G-C content resulting almost insulating property. However, overall device performances are improved by introduction of G-C rich DNAs in rr-PQT-12. It is due to hot carrier injection phenomenon by donor rr-PQT-12 similar to earlier report [Beratan et al. (2016)]. An increasing trend in the Φ_B is observed with increasing content of either case of G-C rich DNAs (both ss- or ds-DNA) results reduction in current density. It means that S2 or D2 concentrations of DNAs are optimal for better device performance. Thus, on comparing all parameters, ITO/D2/rr-PQT-12 device exhibit enhancement in the charge transport than ITO/S2/rr-PQT-12 (turn-on voltage =0.556 V *vs.* 0.628 V, η= 3.05 *vs.* 3.21and RR =1890 *vs.* 904). This is due to rigid structure of ds-DNA that favors more carrier transport from nucleobases after the injection of carriers by donor rr-PQT-12. This conclusion can also be exemplified from log J-log V plot as shown in Fig. 5.8. In general, fibrous rr-PQT-12 composes of three well explained regions designated as A, B and C corresponding to Ohmic, trap-filling/trap-limited space charge limited current and trap-free space charge limited current regions respectively [Gupta et al. (2011), Singh et al. (2017), Nikitenko at al. (2003)]. Except slope nature, both ITO/D2/rr-PQT-12/Al and ITO/S2/rr-PQT-12/Al possess all these three regions. Particularly, region B, B' or B'' regions are described by power law, in which it is assumed that filling of trap distribution occur exponentially and are of maximum density near the band edge. Since the order of slope increasing from B→B'→B'' i.e. 1.89, 1.99 and 2.39 respectively, therefore trap-filling distribution can be assumed as abruption case of B'', results from favorable injection of carriers causing fast transition rate. Further it is believed that, approximately all trapping

centers are occupied by injected charge carriers on/after the intersection of B'' and C''-regions [Nikitenko at al. (2003), Chiguvare et al. (2004)] and current density increases exponentially with short applied voltage range (the detailed mechanism related to trap distribution has been reported earlier[Singh et al. (2017)]).

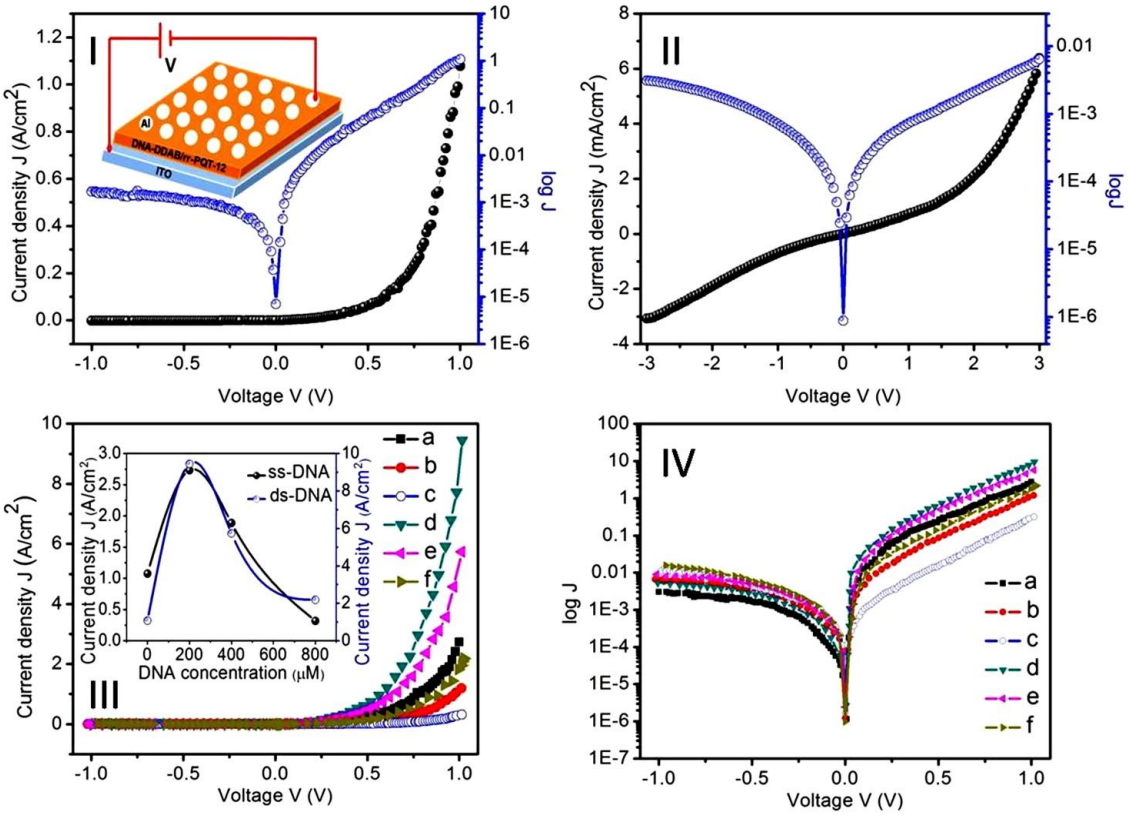

Fig. 5.7. J-V characteristics of (I) rr-PQT-12 (II) ND/rr-PQT-12 and (III) S2/rr-PQT-12, S4/rr-PQT-12, S8/rr-PQT-12, D2/rr PQT-12, D4/rr-PQT-12 and D8/rr-PQT-12 (a-f) and log J-V plot of (IV) S2/rr-PQT-12, S4/rr-PQT-12, S8/rr-PQT-12, D2/rr-PQT-12, D4/rr-PQT-12 and D8/rr-PQT-12 (a-f). Inset pictures of **Fig. 5.7** (I & III), represents the fabricated device schematic and variation of current density (J) with DNA contents in respective composites respectively.

The stability of both devices were examined for its RR value till 15 days with an interval of 5 days in ambient conditions and found that the RR value of ITO/D2/rr-PQT-12 and ITO/S2/rr-PQT-12 devices are sustained to ~75% and ~ 65% respectively (*cf.* Fig. 5.9).

Table. 5.1. Various parameters associated with different samples excited at wavelength 369 nm.

Fluorescent system at different steps of modification	τ_1(std.dev.) nanoseconds	τ_2(std.dev.) nanoseconds	B1(std.dev.)	B2(std.dev.)	% of τ_1	% of τ_2	χ^2
rr-PQT-12	0.47(0.01)	0.76(0.02)	0.041(0.002)	0.013(0.003)	65.37	34.63	1.127
S2/rr-PQT-12	0.54(0.01)	0.86(0.08)	0.047(0.001)	0.004(0.002)	87.32	12.68	1.079
D2/rr-PQT-12	0.54(0.01)	0.94(0.08)	0.049(0.001)	0.003(0.001)	90.76	9.24	1.089

Table 5.2. Device parameters of all materials

Devices	Barrier Height Φ_B (eV)	Turn-on Voltage T_{ON} (V)	Saturation Current Density J_0 (A/cm^2)	Ideality Factor (η)	Rectification Ratio RR (-1.0 to 1.0 V)
ITO/rr-PQT-12/Al	0.705±0.045	0.73	$(1.81\pm0.11)\times10^{-5}$	4.03	629
ITO/ND/rr-PQT-12/Al**	0.789±0.038	1.98	$(8.76\pm0.15)\times10^{-7}$	28.42	2
ITO/S2/rr-PQT-12/Al	0.625±0.024	0.63	$(3.97\pm0.13)\times10^{-4}$	3.91	904
ITO/S4/rr-PQT-12/Al	0.668±0.028	0.71	$(7.56\pm0.11)\times10^{-5}$	3.89	198
ITO/S8/rr-PQT-12/Al	0.745±0.029	0.88	$(3.87\pm0.18)\times10^{-6}$	4.54	31
ITO/D2/rr-PQT-12/Al	0.578±0.021	0.56	$(2.38\pm0.09)\times10^{-3}$	3.05	1890
ITO/D4/rr-PQT-12/Al	0.601±0.027	0.65	$(1.01\pm0.06)\times10^{-3}$	3.71	716
ITO/D8/rr-PQT-12/Al	0.669±0.020	0.69	$(7.25\pm0.19)\times10^{-5}$	3.65	137

** The device parameters were calculated with applied voltage range from -3.0 to +3.0 V.

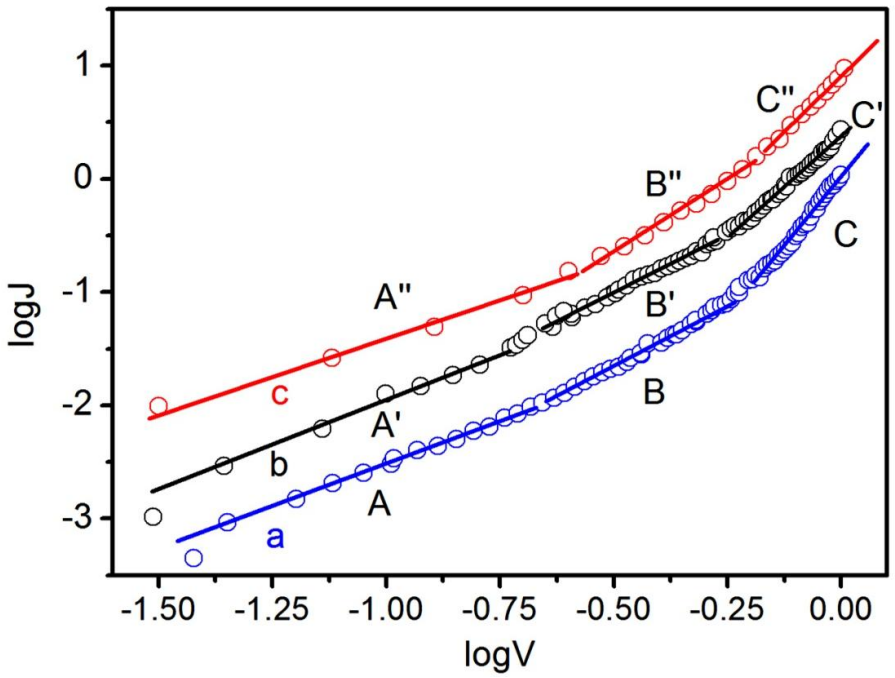

Fig. 5.8. log J-log V plot of (a) ITO/rr-PQT-12/Al, (b) ITO/S2/rr-PQT-12/Al and (c) ITO/D2/rr- PQT-12/Al devices.

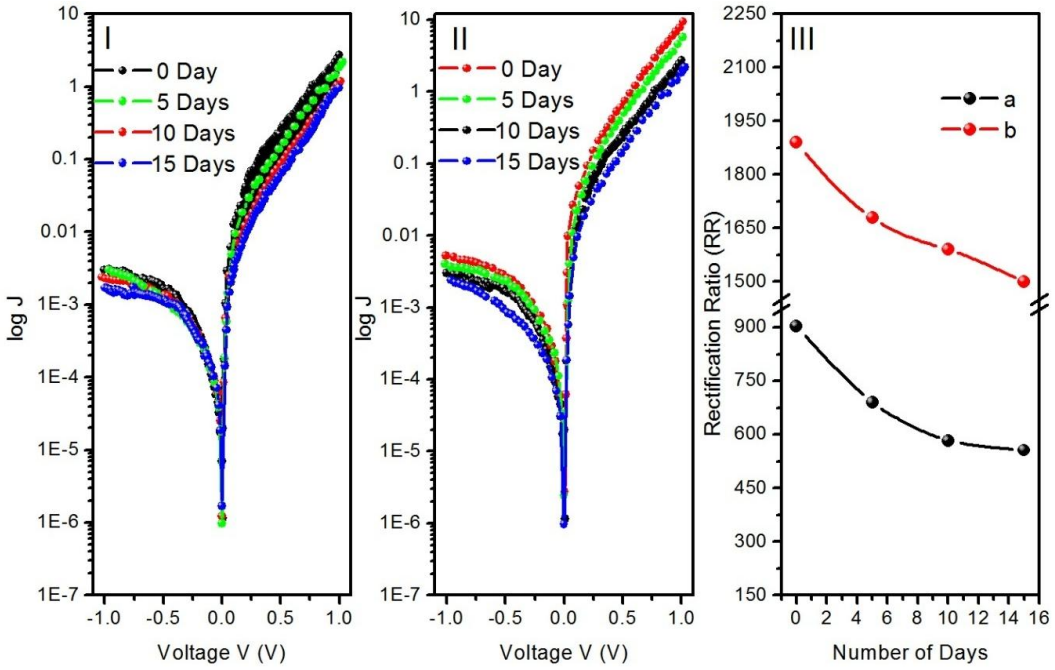

Fig. 5.9. Time dependent device performance of (I) S2/rr-PQT-12 (II) D2/rr-PQT-12 and (III) combined RR *vs.* number of days plot for (a) S2/rr-PQT-12 & (b) D2/rr-PQT-12 based devices.

5.4 Conclusion

The DNA-polymer complex formation was done for device prospects with very facile method probably for the first time where DNA-DDAB complexes were successfully prepared in aqueous media which is hydrophobic in nature and used as template to orient the rr-PQT-12 through weak edge-on manner over the complex in chloroform solution. However; face-on orientation is prominent between polymer chains due to its planer and rigid backbone. So conduction in the DNA templated fibrous polymer, is taking place via both face-on and edge-on aggregates. This as-prepared fibrous material is ~100 nm in size (diameter) when aggregated over DNA. The devices fabricated using DNA incorporated in rr-PQT-12 exhibit higher rectification ratio (1.43 times in the case of ss-DNA and 3.04 times in the case of ds-DNA) than that of polymer alone due to charge carrier injection by assembled polymer to nearby nucleobases. The device having structure ITO/D2/rr-PQT-12, exhibits better charge transport properties than that of ITO/S2/rr-PQT-12 and other counterparts. This is due to rigid ds-DNA that favours more carrier transport from nucleobases after the injection of carriers by donor rr-PQT-12 (as shown in Fig. 5.1 (II)). Further such synthesis approach of polymer assembly over the template that possess the concept of charge injection phenomenon can be extended for other polymer variants and also may be explored for other applications such as catalysis, sensors, and electronic applications (OFETs).